



HERSCHEL EXTREME LENSING LINE OBSERVATIONS: [C II] VARIATIONS IN GALAXIES AT REDSHIFTS $z = 1-3^*$

SANGEETA MALHOTRA¹, JAMES E. RHOADS¹, K. FINKELSTEIN², HUAN YANG¹, CHRIS CARILLI³, FRANÇOISE COMBES⁴,
 KARINE DASSAS⁵, STEVEN FINKELSTEIN², BRENDA FRYE⁶, MARYVONNE GERIN⁷, PIERRE GUILLARD⁵, NICOLE NESVADBA⁵,
 JANE RIGBY⁸, MIN-SU SHIN⁹, MARCO SPAANS¹⁰, MICHAEL A. STRAUSS¹¹, AND CASEY PAPOVICH¹²

¹School of Earth and Space Exploration, Arizona State University, Tempe, AZ 85287, USA; malhotra@asu.edu

²University of Texas, Austin, TX 78712, USA

³National Radio Astronomy Observatory, Socorro, NM, USA

⁴Observatoire de Paris, LERMA, CNRS, 61 Avenue de l'Observatoire, F-75014 Paris, France

⁵Institut d'Astrophysique Spatiale, Centre Universitaire d'Orsay, France

⁶Steward Observatory, University of Arizona, Tucson, AZ, USA

⁷LERMA, 24 rue Lhomond, F-75231 Paris Cedex 05, France

⁸NASA, Goddard Space Flight Center, Greenbelt, MD, USA

⁹Oxford University, Oxford, OX1 3PA, UK

¹⁰Kapteyn Astronomical Institute, University of Groningen, Groningen, The Netherlands

¹¹Department of Astrophysical Sciences, Princeton University, Peyton Hall, Princeton, NJ 08544, USA

¹²George P. and Cynthia W. Mitchell Institute for Fundamental Physics and Astronomy, Department of Physics, Texas A&M University, College Station, TX 77843, USA

Received 2013 August 21; revised 2016 August 29; accepted 2016 September 6; published 2017 January 20

ABSTRACT

We observed the [C II] line in 15 lensed galaxies at redshifts $1 < z < 3$ using HIFI on the *Herschel Space Observatory* and detected 14/15 galaxies at 3σ or better. High magnifications enable even modestly luminous galaxies to be detected in [C II] with *Herschel*. The [C II] luminosity in this sample ranges from $8 \times 10^7 L_\odot$ to $3.7 \times 10^9 L_\odot$ (after correcting for magnification), confirming that [C II] is a strong tracer of the ISM at high redshifts. The ratio of the [C II] line to the total far-infrared (FIR) luminosity serves as a measure of the ratio of gas to dust cooling and thus the efficiency of the grain photoelectric heating process. It varies between 3.3% and 0.09%. We compare the [C II]/FIR ratio to that of galaxies at $z = 0$ and at high redshifts and find that they follow similar trends. The [C II]/FIR ratio is lower for galaxies with higher dust temperatures. This is best explained if increased UV intensity leads to higher FIR luminosity and dust temperatures, but gas heating does not rise due to lower photoelectric heating efficiency. The [C II]/FIR ratio shows weaker correlation with FIR luminosity. At low redshifts highly luminous galaxies tend to have warm dust, so the effects of dust temperature and luminosity are degenerate. Luminous galaxies at high redshifts show a range of dust temperatures, showing that [C II]/FIR correlates most strongly with dust temperature. The [C II] to mid-IR ratio for the HELLO sample is similar to the values seen for low-redshift galaxies, indicating that small grains and PAHs dominate the heating in the neutral ISM, although some of the high [C II]/FIR ratios may be due to turbulent heating.

Key words: infrared: ISM – ISM: atoms – galaxies: high-redshift – radiation mechanisms: thermal

1. INTRODUCTION

The fine structure line of C^+ ($157.74 \mu\text{m}$) is a major coolant of the neutral interstellar medium, because it has the right energy gap ($\Delta E/k = 91 \text{ K}$) for excitation by warm gas. Carbon has a lower ionization potential (11.26 eV) than hydrogen, so that carbon can be in the form of C^+ in diffuse neutral hydrogen clouds and on the surface of UV-illuminated gas clouds. Carbon is also the fourth most abundant atom. Thus, C^+ can cool warm neutral gas where the two most abundant atoms, H and He, cannot (see Tielens & Hollenbach 1985; Wolfire et al. 1990; hereafter, TH85 and WTH90).

The [C II] line is roughly 1300 times as intense as the CO(1 \rightarrow 0) rotational line in normal galaxies and Galactic molecular clouds and 4100 times as intense as the CO(1 \rightarrow 0) line in starburst nuclei and Galactic star formation regions (Crawford et al. 1985; Stacey et al. 1991). For normal galaxy nuclei and star formation regions in the spiral arms, most of the observed [C II] arises from photon-dominated regions (PDRs)

on molecular cloud surfaces. However, integrated over the disks of normal spiral galaxies, a substantial fraction of [C II] emission may also arise from “standard” atomic clouds, i.e., the cold neutral medium (CNM; Madden et al. 1993); from extended, low-density ionized regions (Heiles 1994); or from CO-dark molecular hydrogen extending over large parts of the Galactic disk and in the halos of galaxies (Contursi et al. 2013; Pineda et al. 2013).

For most galaxies, 0.1%–1% of the far-infrared (FIR) continuum emerges in the [C II] line. Not coincidentally, it is the best studied line in this wavelength regime. It has been observed for normal galaxies (Stacey et al. 1991; Malhotra et al. 1997, 2001; Leech et al. 1999; Pierini et al. 1999), irregular and dwarf galaxies (Smith & Madden 1997; Bergvall et al. 2000; Hunter et al. 2001; Madden 2001), ellipticals (Malhotra et al. 2000; Unger et al. 2000), luminous infrared galaxies (Graciá-Carpio et al. 2011; Díaz-Santos et al. 2013, 2014), and ultraluminous infrared galaxies (ULIRGs) (Luhman et al. 1998; Fischer 2000; Farrah et al. 2013).

Thus, the [C II] ($158 \mu\text{m}$) line is a bright line in the submillimeter range useful for the determination of redshifts and kinematics of gas (Carilli & Walter 2013; Rhoads et al.

* *Herschel* is an ESA space observatory with science instruments provided by European-led Principal Investigator consortia and with important participation from NASA.

2014). Combined with the measurement of the FIR continuum and other cooling lines, it is a good diagnostic of physical conditions in gas near star-forming regions (Kaufman et al. 1999; Malhotra et al. 2001).

The energy radiated through [C II] line cooling must be balanced by the heating of the PDRs, CNM, and WNM. This gas is heated primarily by the ejection of energetic photoelectrons from dust grains that absorb UV photons (Watson 1972). These photoelectrons carry a small fraction of the incident UV photon energy, while the grains re-emit the majority of their absorbed light energy as an FIR continuum. Thus, the ratio of energy in the [C II] line to the total FIR dust continuum emission serves as a measure of the efficiency of the photoelectric heating of neutral gas, which is why we expect this ratio to be fairly constant. This was seen in samples of nearby galaxies (e.g., Stacey et al. 1991) with the Kuiper Airborne Observatory. With the *Infrared Space Observatory* (*ISO*) mission, surveys of large samples of galaxies were carried out, and the ratio of [C II]/FIR was seen to vary by a factor of 50 by Malhotra et al. (1997) and Luhman et al. (1998), decreasing dramatically both for galaxies with high average dust temperatures (as measured by F60/F100) and for ULIRGs. Values of $L_{[\text{C II}]} / L_{\text{FIR}}$ higher than allowed by photoelectric effect heating are seen in gas that is shock heated (e.g., Appleton et al. 2013).

The [C II] line has been observed for sources with high redshifts, up to $z = 7$ (Venemans et al. 2012). Galaxies at high redshift do not all show a deficiency of [C II] at high FIR luminosities (Iono et al. 2007; Maiolino et al. 2009; Stacey et al. 2010; Capak et al. 2015). It is possible—even likely—that physical conditions in the star-forming interstellar medium in high-redshift galaxies are different from those in low-redshift galaxies. We know that the volume-averaged star formation rate (SFR) peaks at $z = 2$. There are observations to indicate that $z = 2$ starburst galaxies have thicker, more turbulent disks (Förster Schreiber et al. 2009) and larger starburst regions (e.g., Hailey-Dunsheath et al. 2010; Rujopakarn et al. 2011). Low-metallicity dwarf galaxies at low z show somewhat elevated [C II]/FIR ratios (e.g., Cormier et al. 2010; Hunter et al. 2001; Israel & Maloney 2011) and dramatically elevated [C II]/CO ratios. If the starbursts at high redshifts are indeed like the local irregular galaxies—e.g., the LMC, SMC, and IC 10—we should see higher [C II]/FIR ratios. With the *Herschel Space Observatory*, [C II] lines have been detected for high-redshift galaxies ($z \simeq 2$), but the galaxies studied so far at $z > 1$ have been ULIRGs and hyperluminous IR galaxies (HyLIRGs).

We report on [C II] observations of 15 strongly lensed galaxies at redshifts $1 < z < 3$. High magnification factors allow us to study galaxies that have SFRs and FIR luminosities typical of the most common galaxies. The [C II] line observations were done with the Heterodyne Instrument for the Far-Infrared (HIFI; de Graauw et al. 2010) on the *Herschel Space Observatory* (Pilbratt et al. 2010). Section 2 describes the sample of high-redshift galaxies in the *Herschel* Extreme Lensing Line Observations (HELLO) project (Section 2.1), the [C II] line observations (Section 2.2), and the data analysis (Section 2.3). In Section 3 we analyze the variation of [C II]/FIR with FIR luminosity and dust temperature, and in Section 4 we discuss the astrophysical implications of our findings. Section 5 presents our conclusions and a summary of the main results.

2. OBSERVATIONS

2.1. The Sample

The HELLO sample is a set of 15 lensed galaxies at redshifts $1.0 < z < 3.0$ selected to be a representative set of star-forming galaxies with modest intrinsic luminosities and high magnification factors. They are well-studied objects, thanks to their apparent brightness. All have multiwavelength imaging, often including *Hubble Space Telescope* observations. All have published redshifts from optical and/or mm-wave spectroscopy. Many also have published SFRs, metallicities, and detailed lens models.

To construct the sample, we combed the literature for well-characterized lens systems at redshifts and flux levels suitable for *Herschel* HIFI [C II] line observations. We prioritized sources where we could also hope to measure the [O I] 63 μm line using PACS spectroscopy—a part of the HELLO survey that we will describe in a separate publication. We gave some preference to sources with well-measured 24 μm fluxes (rest-frame 8–12 μm), since this provides one of the better predictors of the expected [C II] brightness (Helou et al. 2001) and so reduces uncertainties in observation planning. We rejected sources with indications of energetically dominant active galactic nuclei. Thirteen of the 15 galaxies in this sample were initially found in optical surveys, including 9 from Sloan Digital Sky Survey (SDSS) imaging. The remaining two are submillimeter-identified sources. Six are lensed by massive galaxy clusters, and the remaining nine by galaxy groups or individual galaxies.

A final cut was applied to the sample to select sources where the redshift is known to a precision of 10^{-3} , in order to tune the HIFI spectral range properly. The final sample had published intrinsic SFRs varying between ~ 1500 and $\sim 3 M_{\odot} \text{yr}^{-1}$ and magnifications of $4 \lesssim \mu \lesssim 60$. We list the sample objects and summarize key characteristics in Table 1.

2.2. [C II] Line Observations

We observed the high-redshift [C II] lines using HIFI on *Herschel*. To get the maximum bandwidth, we used the Wide Band Spectrometer, which has a bandwidth of 4 GHz and a resolution of 1 Mhz. For our redshift range, the line falls in receiver band 1, 2, or 3. Nearly all our sources are spatially unresolved for HIFI, which has a half-power beam width of 44'' for band 1, 33'' for band 2, and 26''.5 for band 3 (Roelfsema et al. 2012). There is a very low probability of any other sources contaminating the line signal, as the bandwidth is less than one percent.¹³ To maximize baseline stability, the observations were made in the fast-chop, dual-beam switch mode.

Our total HIFI observing times ranged from ~ 3100 to $\sim 14,200$ s per source, with an on-source integration time of ~ 970 to ~ 3300 s. The integration times were chosen based on the instrument sensitivity at the relevant redshifted frequency, combined with a preliminary estimate of the likely [C II] flux. This estimate was in turn based on correlations with mid-infrared observations with *Spitzer* and/or FIR fluxes derived from SFRs. For lensed sources with published mid-IR fluxes (Rigby et al. 2008; Fadely et al. 2010; Rujopakarn et al. 2012),

¹³ The sole exception to both statements is SMMJ163554.2+661225. Here, one of the three lensed images lies outside the HIFI beam, and one other known source at nearly identical redshift is within the beam (Kneib et al. 2004).

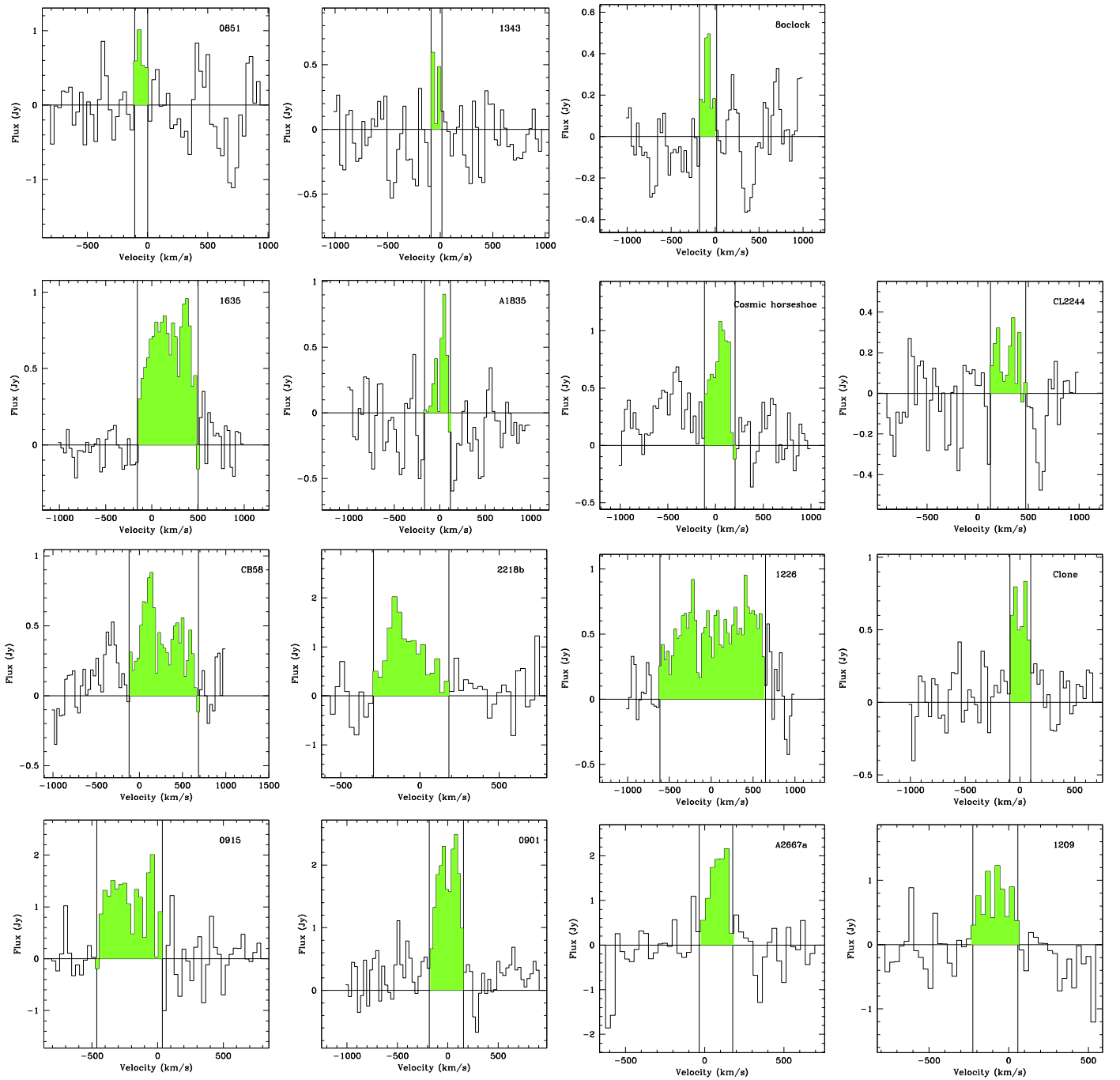


Figure 1. [C II] Spectra of the HELLO sample with HIFI aboard *Herschel*. The line profiles have been boxcar-smoothed to 40 km s^{-1} . We see a variety of line profiles ranging from double-horned profiles indicating rotation in 0901 (Rhoads et al. 2014) to large line widths, possibly indicating outflows in CB58. The velocity extent of the line is indicated by the shaded region. The velocities are relative to published redshifts, mostly from optical spectroscopy, given in Table 1. Fluxes were measured in mK and converted to Jy, following the HIFI calibrations provided by Roelfsema et al. (2012).

we used the scaling derived from the correlation between mid-IR ($8 \mu\text{m}$) fluxes and [C II] (Helou et al. 2001). For sources which did not have mid-IR observations, we used the published values of SFRs and converted them to FIR luminosities (Kennicutt 1998). The desired [C II] sensitivity limit (4σ) was then set to be 1×10^{-3} of the FIR luminosity estimate.

2.3. Data Analysis

We started the data reduction with level-2 products from HIFI. The spectrum for each polarization was stitched and then

smoothed to 40 km s^{-1} . Second-order baselines were subtracted after excluding the expected frequency range of the [C II] line. After that we coadded spectra from both H and V polarizations to obtain the final spectrum. All of this processing was done in the *Herschel* Interactive Pipeline Environment (HIPE v9.2). The one-dimensional spectra were then written out as ASCII files and manipulated outside HIPE. The resulting spectra are shown in figure 1. The [C II] line fluxes were derived by directly integrating the flux seen in a fiducial line centered on the expected frequency. Given that [C II] line shapes are complex and non-Gaussian, arising from the rotation

Table 1
[C II]/FIR for the HELLO Sample Galaxies

Name	Redshift	R.A.	Decl.	μ	L_{FIR}^a $\times 10^{11} L_{\odot}$	SFR ($M_{\odot} \text{ yr}^{-1}$)	$\frac{F_{60}}{F_{100}}$ F100	[C II] ($\times 10^{-18} \text{ W m}^{-2}$)	$\frac{L_{\text{[C II]}}}{L_{\text{FIR}}}$ ($\times 10^{-3}$)	References
Abell 2667a	1.0334	23 ^h 51 ^m 40.00	-26 ^d 04 ^m 52.0	17	1.1	36.9	0.55	9.4 ± 1.2	7.3	1
Cosmic Horseshoe	2.3811	11 ^h 48 ^m 33.14	19 ^d 30 ^m 03.2	24	1.0	32.8	1.25 ^b	3.0 ± 0.7	14.5	6
Abell 2218b	1.032	16 ^h 35 ^m 55.16	66 ^d 11 ^m 50.8	6.1	1.7	54.7	0.74	11.3 ± 1.4	12.6	3
The Clone ^c	2.003	12 ^h 06 ^m 01.82	51 ^d 42 ^m 30.5	28	1.7	56	0.68	2.1 ± 0.3	3.3	4
8 O'Clock Arc	2.728	00 ^h 22 ^m 40.80	14 ^d 31 ^m 13.8	12.3	14.7	477	1.04	1.0 ± 0.3	0.90	5
SMMJ14011 (A1835)	2.5653	14 ^h 01 ^m 04.94	02 ^d 52 ^m 25	3.6	26.7	866	0.82	1.8 ± 0.5	2.6	6
SDSS 090122+181432	2.2558	09 ^h 01 ^m 22.37	18 ^d 14 ^m 32.4	8	48.11	1560	0.62	10.4 ± 0.4	2.75	7
Abell 2218 ^d	2.515	16 ^h 35 ^m 54.18	66 ^d 12 ^m 24.8	22	4.8	155	0.79	7.4 ± 1.1	9.43	8
MS1512-cB58 ^e	2.7265	15 ^h 14 ^m 22.27	36 ^d 36 ^m 25.2	30	3.1	100	1.21	4.7 ± 0.4	8.3	9
SDSS J085137+333114	1.6926	08 ^h 51 ^m 37.11	33 ^d 31 ^m 14	27	0.9	29.	0.42	2.0 ± 0.6	4.0	10
SGASJ122651+215220 ^f	2.9233	12 ^h 26 ^m 51.55	21 ^d 52 ^m 14.4	40	1.3	43.7	1.4 ^b	9.3 ± 0.8	33.5	10, 11
SDSS134332+415503	2.0927	13 ^h 43 ^m 33.7	41 ^d 55 ^m 08	40	0.5	18.0	...	0.9 ± 0.3	3.5	7, 15
SDSSJ120924+264052	1.021	12 ^h 09 ^m 24.34	26 ^d 40 ^m 52.44	58	<0.08	<2.8	...	7.8 ± 1.1	>7.4	12
SDSSJ091538+382658	1.501	09 ^h 15 ^m 38.15	38 ^d 27 ^m 05 ^m	25	<0.45	<14.5	...	13.8 ± 0.6	>15.3	13
CL 2244	2.237	22 ^h 47 ^m 11.73	-2 ^d 05 ^m 40.3	20	<0.6	<19	...	1.4 ± 0.5	...	14

Notes.

^a The L_{FIR} and SFR tabulated here have been corrected for the magnification estimates given in column 5. The last three sources in the table are undetected in our PACS/SPIRE images. For these the L_{FIR} is based on 3σ upper limits.

^b The 60/100 μm flux ratios for the Cosmic Horseshoe and SDSS J122651.3+215220 are substantially uncertain.

^c Also known as SDSS J120602.09+514229.5.

^d Also known as SMM J163554.2+661225.

^e Also known as cB58.

^f There is a $\sim 7''$ discrepancy between the coordinates reported in the discovery paper (Koester et al. 2010) and in later followup (Bayliss et al. 2011). We tabulate this object with its original name and with the best coordinates we could find, and note that both positions are well within the same HIFI beam.

References. (1) Rujopakarn et al. (2012), (2) Belokurov et al. (2007), (3) Pello-Descayre et al. (1988), (4) Lin et al. (2009), (5) Allam et al. (2007), (6) Frayer et al. (1999), (7) Diehl et al. (2009), (8) Kneib et al. (2004), (9) Yee et al. (1996), (10) Bayliss et al. (2011), (11) Koester et al. (2010), (12) Ofek et al. (2008), (13) Bayliss et al. (2010), (14) Mellier et al. (1991), (15) Saintonge et al. (2013).

and outflow/inflow motions of the ISM (e.g., Contursi et al. 2013; Rhoads et al. 2014), this method is independent of the kinematical models of [C II] motions. The biggest uncertainty comes from a lack of prior knowledge of the line width in many cases. We examined the smoothed spectra and set the limits of integration at the frequencies where the flux goes to zero on either side of the central frequency. Measurement errors in the line flux were estimated by integrating line fluxes centered at random frequencies in the spectrum (after excluding channels with signals), using the same line width as for actual measurements. The advantage of this approach is that we do not have to assume that the binned data are independent or that the noise goes down as $1/\sqrt{n}$, where n is the number of bins. The [C II] line fluxes and the measurement errors on these fluxes are listed in Table 1.

The FIR continuum was measured with PACS (Poglitsch et al. 2010) and SPIRE (Griffin et al. 2010) imaging. We obtained PACS imaging under the HELLO program for three sources (SDSS J085137+333114, SDSS J091538+382658, and SDSS J120924+264052) plus SPIRE imaging for the last two. For other sources, we used archival PACS and SPIRE imaging data from other *Herschel* programs. The data were reduced using standard procedures with HIPE.

For PACS photometry we used HIPE version 10.0 to reduce the data from the raw products (level 0) to a fully calibrated map (level 2). We used standard pipeline routines as described in the online PACS data reduction guides. We used the official Python scripts for the PACS ‘‘Bright Point Source Scan Map’’ and ‘‘Multiple ObsID Scan Map Bright Point Source,’’ and we employed the recommended method of using ‘‘HighPassFilter’’ to remove large-scale artifacts. The bright sources at the center

of the map were masked out prior to filtering, and the size of the mask was chosen to be less than or equal to the high-pass filter’s size so that none of the source flux was removed but as much of the $1/f$ noise as possible was removed without damaging the point-spread function. The individual AORs for each PACS source were combined into a final mosaic. Typically there were two image sets that went into each of the PACS 70 and 100 μm mosaic images, and four images that were combined for the final PACS 160 μm mosaic. Aperture photometry was performed on the final mosaics to measure the flux of the lensed sources, and standard aperture corrections were applied. The aperture photometry was done with both Source Extractor (Bertin & Arnouts 1996) and the IDL ‘‘aper’’ package. In cases where a source was undetected and could not be extracted using SExtractor, ‘‘aper’’ was used to estimate an upper limit at the source location. Errors were estimated by placing random apertures on sky locations in the images.

SPIRE fluxes were derived from Level 2 maps processed with HIPE (version 10.0.2747), with standard corrections for instrumental effects and glitches. Striping induced by offsets in the flux calibration from one detector to another was removed using the Scan Map Destriper module included in HIPE. The fluxes were derived from the map using simple point source photometry. Errors were derived by placing random such apertures on the map, which gives error estimates, including those due to confusion noise, a dominant component in most cases (Nguyen et al. 2010).

We used the PACS 100 and 160 μm fluxes and SPIRE 250, 350, and 500 μm fluxes to derive the FIR continuum spectral energy distribution of each source. The foreground lensing galaxies do not contribute significantly to the FIR continuum,

Table 2
[C II]/FIR Ratios of High-redshift Galaxies from the Literature

Name	Redshift	L_{FIR}	F60/F100	$F_{[\text{C II}]} / L_{\text{FIR}}$	References
61.1	4.42	$2.1 \times 10^{12} L_{\odot}$	0.6	$7.1\text{e-}4$	Swinbank12
65.1	4.44	$2.0 \times 10^{12} L_{\odot}$	0.6	$1.6\text{e-}3$	Swinbank12
BR1202-0725N	4.7	$12.0 \times 10^{12} L_{\odot}$	1.4	$8.3\text{e-}4$	Wagg12
BR1202-0725S	4.7	$26 \times 10^{12} L_{\odot}$	1.4	$2.5\text{e-}4$	Wagg12
SP 81	3.0	$5.7 \times 10^{12} L_{\odot}$	0.7	$5.6\text{e-}3$	Valtachnov11
SMMJ2135	2.3	$2.3 \times 10^{12} L_{\odot}$	0.74	$2.4\text{e-}3$	Iverson10
ID141	4.24	$8.5 \times 10^{12} L_{\odot}$	0.8	$7.3\text{e-}4$	Cox11
SDSS1148	6.42	$22 \times 10^{12} L_{\odot}$	1.6	$2\text{e-}4$	fitted NED data
HyWT	2.41	$34 \times 10^{12} L_{\odot}$	0.65	$1\text{e-}3$	Iverson et al. (2013)
HFLS3	6.3	$28.6 \times 10^{12} L_{\odot}$	0.94	$5.4\text{e-}4$	Riechers et al. (2013)
MIPSJ1428	1.23	$3 \times 10^{12} L_{\odot}$	0.76	$2\text{e-}3$	Hailey-Dunsheath et al. (2010)

because they are early-type galaxies and are at lower redshifts. So we expect very little dust in these galaxies, which should peak between 60 and $100 \times (1 + z_{\text{lens}}) \mu\text{m}$, where $z_{\text{lens}} \sim 0.2-0.5$; whereas the lensed sources should peak at $\approx 100 \times (1 + z)$ microns. We un-redshifted the SEDs back to the source restframe and spline-fit a smooth curve through the observations while resampling the fluxes to $5 \mu\text{m}$ intervals. Then we estimated the fluxes that would be seen in IRAS-like filters at restframe 60 and $100 \mu\text{m}$. This procedure has the advantage of estimating/interpolating the restframe 60 and $100 \mu\text{m}$ fluxes for direct and fair comparison with $z = 0$ samples in a model-independent way. The FIR flux was calculated as $F_{\text{FIR}} = 1.26 \times 10^{-14} [2.58 \times F_{\nu}(60 \mu\text{m}) + F_{\nu}(100 \mu\text{m})] \text{W m}^{-2}$ (Helou et al. 1988), where $F_{\nu}(60 \mu\text{m})$ and $F_{\nu}(100 \mu\text{m})$ are the flux densities in jansky at 60 and $100 \mu\text{m}$. This gives a flux between 40 and $120 \mu\text{m}$. We checked the derived fluxes for three sources previously published by Magnelli et al. (2012) and Finkelstein et al. (2011). These authors define $L(\text{FIR})$ to be the dust continuum between 8 and $1000 \mu\text{m}$. Their luminosities and ours between rest wavelengths of $40-120 \mu\text{m}$ should differ by a factor of 1.9 according to the models of Dale et al. (2001), whereas we found a ratio between 1.7 and 2.1 between our luminosities and those of Magnelli et al. (2012). This is reasonable considering the random measurement errors and the dependence on models for converting flux to luminosity.

3. RESULTS

In the HELLO project we observed 15 galaxies that are more typical of the star-forming galaxies at $z \sim 2$. Strong lensing gives us the much needed boost to make the [C II] line and FIR continuum detectable with *Herschel*. Of the 15 sources, 14 were detected at S/N of 3 or better; CL2244 was a marginal detection at 2.8σ . The main uncertainty in the [C II] flux and detections is due to an unknown velocity width of the line.

One source, CL2244, was not detected in either the continuum or the [C II] line. Of the remaining 14 sources, we consider SDSS 134332+415503.4 to be a marginal detection primarily because the line seems very narrow (107 km s^{-1}) and we do not have an independent verification of the line width for this source. The other 13 sources are well detected with HIFI. Two of these—SDSS J091538+382658 and SDSS J120924+264052—are not detected with PACS/SPIRE imaging, leading to lower limits on [C II]/FIR. For the Cosmic Horseshoe and SDSS J122651.3+215220, PACS/SPIRE fluxes lead to uncertain values of FIR colors F60/F100. In Table 1, we also calculate the SFR from the FIR luminosity

using the relation given by Kennicutt (1998): $\text{SFR}(M_{\odot} \text{ yr}^{-1}) = 4.5 \times 10^{-44} L(\text{FIR})(\text{erg s}^{-1})$. Both the FIR luminosities and the SFRs are corrected for magnification by the magnification factor μ in Table 1.

Thus, we have a sample of 11(9) galaxies for which we can quantify the dependence of [C II]/FIR on FIR luminosity (FIR colors). We augmented this with a sample of 11 galaxies with redshifts $z = 1.3-6.42$ and with [C II] fluxes from the literature (Table 2). This is a subset of a larger sample of high-redshift galaxies with [C II] line detections for which there were continuum detections at multiple wavelengths so we could derive the FIR colors F60/F100. We used a sample of 71 normal and ultraluminous galaxies near redshift zero to serve as a reference. The nearby reference sample was taken from the *ISO* key project on normal galaxies (PI: Helou) spanning a range of FIR luminosities and F60/F100 colors (Malhotra et al. 2001) and from the Luhman et al. (2003) sample of ULIRGs, which spans a range of luminosities and other FIR properties of ULIRGs.

We see a large variation in the ratio [C II]/FIR in the HELLO sample—from 9×10^{-4} to $\geq 3 \times 10^{-2}$. Three galaxies show [C II]/FIR $> 1\%$, a value three times as high as the modal value of [C II]/FIR at low redshifts (Malhotra et al. 1997, 2001). In these three galaxies—SDSS1226, SDSS 1209, and SDSS 0915—the continuum is not detected in PACS and SPIRE images. Only the [C II] line is detected.

In Figure 2 we plot [C II]/FIR against FIR luminosity. While the low-redshift sample (black squares) shows a decline of [C II]/FIR with FIR, the high-redshift samples, from HELLO and other high-redshift studies, show a large scatter in [C II]/FIR. This is similar to the observations of Stacey et al. (2010). The correlation coefficient between [C II]/FIR and FIR luminosity is 54% for the low-redshift points in Figure 2. For the high-redshift sources the correlation coefficient is 59%. Stacey et al. (2010) postulate a lack of correlation between [C II]/FIR and FIR for their sample at $z = 1-2$. From that sample, we included MIPSJ1428 (Hailey-Dunsheath et al. 2010) since that has *Spitzer* and SHARC measurements of the continuum to determine the F60/F100 ratio (Borys et al. 2006). We also measured the scatter of points around the best-fit linear relation between [C II]/FIR and FIR. The rms scatter of [C II]/FIR was found to be 0.35 and 0.31 dex for the high-redshift and low-redshift samples respectively. Moreover, the best fit for the high- z sample is quite distinct from the low- z linear relation (Figure 2).

In Figure 3 we see that there is a cleaner and stronger correlation between [C II]/FIR and F60/F100. The [C II]/FIR

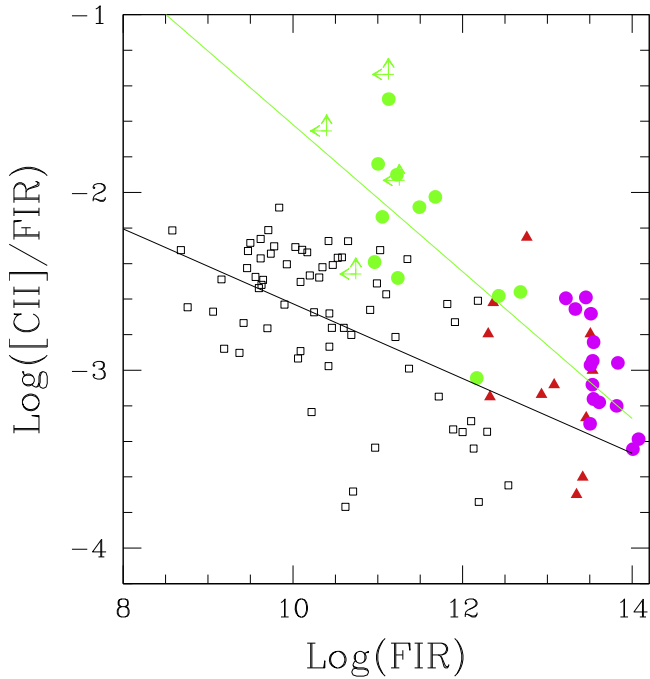


Figure 2. The ratio of the [C II] line to the FIR luminosity is plotted against the FIR luminosity. Black squares denote the low-redshift samples from Malhotra et al. (2001) and Luhman et al. (2003). Green circles denote the HELLO sample of galaxies. Red triangles represent $z > 1$ samples of HyLIRGs and ULIRGs compiled from the literature (table 2). Pink circles are high redshift data from SPT (Gullberg et al 2015). At high redshifts the anticorrelation between [C II]/FIR and FIR luminosity seems to break down, as pointed out by Stacey et al. (2010). We see five cases of [C II]/FIR ratios greater than 1%.

ratio decreases as the FIR color ratio F60/F100 increases due to hotter dust (Figure 3). In our sample we see a full range of $F60/F100 = 0.42\text{--}1.25$. For a modified blackbody dust continuum, these ratios would correspond to dust temperatures between 28 and 46 K for graybody slopes $\beta = 1.5\text{--}2$. Real galaxies, of course, have dust at a range of temperatures, and the F60/F100 ratio can be interpreted as a measure of the average dust temperature or as the distribution of masses of warm versus cold dust. The correlation coefficient between [C II]/FIR and F60/F100 is 70%, higher than the correlation strength seen in Figure 2 between [C II]/FIR and FIR. The rms scatter of [C II]/FIR was found to be 0.29 and 0.37 dex for low and high-redshift samples, which were fit separately. The best-fit lines for the high- z and the low- z linear relation overlap substantially (Figure 3). Any misestimates of magnification factors would affect only the FIR estimates; other quantities, such as [C II]/FIR and F60/F100, are all ratios.

In a previous study of nearby galaxies (Malhotra et al. 1997) pointing out variations of [C II]/FIR, we emphasized the dependence of [C II]/FIR on dust temperature but also saw an anticorrelation between [C II]/FIR and FIR luminosity. The reason for this is that galaxies with higher dust temperatures tend to have higher FIR luminosity (Figure 4). Thus, it was difficult to determine at low redshifts whether [C II]/FIR depends on dust temperature and there is a secondary correlation with FIR luminosity or vice versa. The FIR luminosity and dust temperatures for known high-redshift sources are largely uncorrelated (Figure 4). This makes it possible to determine that the primary correlation is between [C II]/FIR and F60/F100, not luminosity. We postulate that the

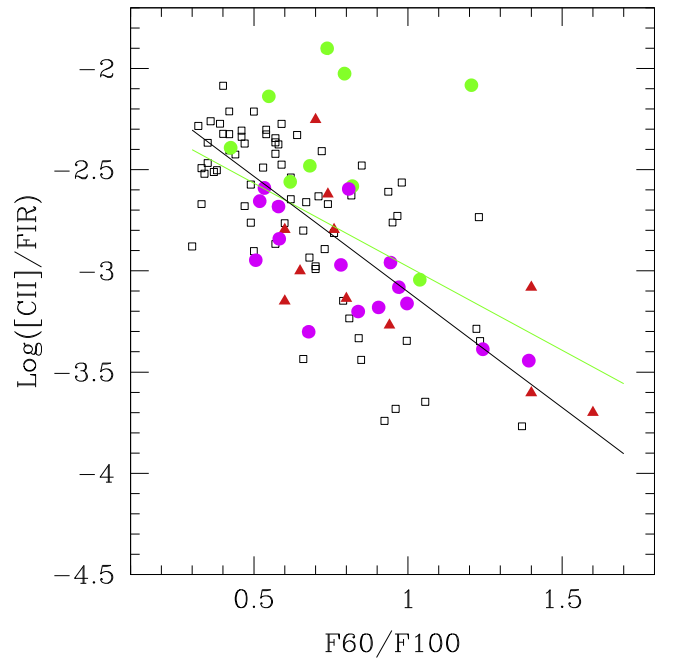


Figure 3. The ratio of the [C II] line to FIR luminosity is plotted against the dust temperature characterized by the ratio of flux densities at 60 and 100 μm . Black squares denote the low-redshift samples from Malhotra et al. (2001) and Luhman et al. (2003). Red triangles represent $z > 2$ samples of HyLIRGs and ULIRGs compiled from literature (table 2); pink circles are high redshift data from SPT (Gullberg et al 2015); and green circles denote the HELLO sample of galaxies. The anticorrelation of [C II]/FIR with F60/F100 is tighter than that with FIR luminosity and seems to hold for both low- and high-redshift galaxies. Sources without FIR continuum detections are not plotted in this figure, since the F60/F100 ratio is unmeasurable for those three sources.

$L_{[\text{C II}]} / L_{\text{FIR}}$ ratio correlates best with dust temperature and not with luminosity, based on the above results: (1) better correlations, (2) lower scatter, and (3) similar behavior at both low and high redshifts. Also, we will see in the next section that there is a good physical explanation for this.

The $z \sim 2$ sample from the HELLO survey shows many galaxies with a high [C II]/FIR ratio. This is consistent with results presented by Brisbin et al. (2015), Stacey et al. (2010), and Capak et al (2015). This could be due to extra heating of the ISM due to turbulence in these galaxies. E.g., Appleton et al. (2013) see it in some low- z galaxies, and high- z galaxies are seen to have highly turbulent media. cB58, 1226, and 1209 all have large velocity widths, perhaps indicative of outflows.

Figure 5 shows [C II]/mid-IR flux ratios for eight galaxies in the HELLO sample for which we have Spitzer fluxes at 24 microns (Rigby et al. 2008, Rujopakarn et al. 2012). These values are compared to local galaxies (Helou et al. 2001). We see that 7/8 HELLO galaxies lie in the range occupied by the local sample, with no dust temperature dependent variation in [C II]/MIR. One galaxy, cB58, shows a higher [C II]/PAH ratio that may be from turbulent heating (e.g. Appleton et al. 2013).

4. DISCUSSION

The observations presented in this paper confirm that the [C II] (158 μm) line is strong at high redshifts, $1 < z < 3$; in many cases stronger than the average trends for local galaxies. It is also reassuring to learn that similar trends are seen at $z = 0$ and $z \approx 2$, implying similar microphysics. What can we learn from the [C II] observations of galaxies, near and far?

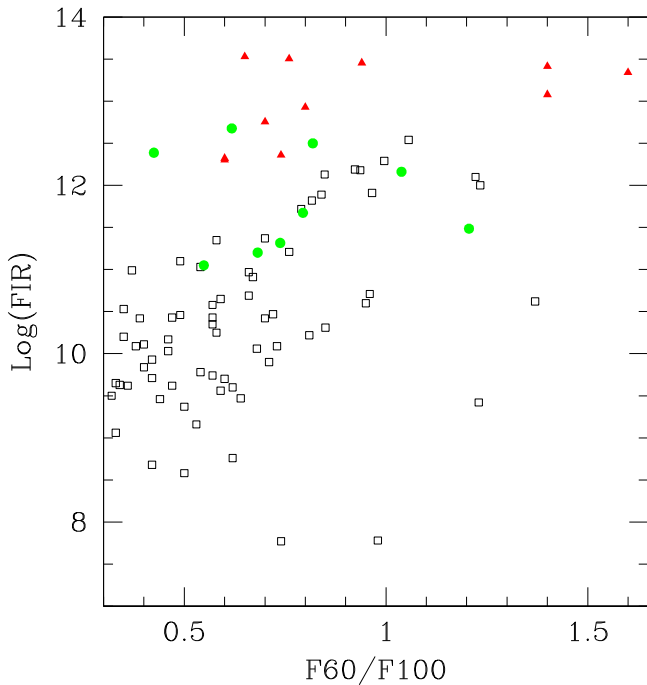


Figure 4. FIR luminosity vs. dust temperature. Black squares denote the low-redshift samples from Malhotra et al. (2001) and Luhman et al. (2003). Red triangles represent the $z > 1$ samples of HyLIRGs and ULIRGs compiled from literature. Green circles denote the HELLO sample of galaxies. At low redshifts, the FIR luminosity and dust temperatures correlate; that is, ULIRGs have warm dust. At high redshifts, the correlation between dust temperature and luminosity vanishes. Some of this could be because colder galaxies are more likely to be selected as submillimeter galaxies (SMGs; see the red points). However, the HELLO sample is largely selected from optical data and should be relatively unbiased in that regard.

The [C II] line has been used as a tracer of the SFR by several studies (e.g., Boselli et al. 2002; de Looze et al. 2011). This is not unreasonable since a large part of the line comes from UV-irradiated dense gas near star-forming regions (PDRs; Crawford et al. 1985). Empirically, it has been shown to correlate with other tracers of star formation as long as star formation is modest. Using [C II] as an SFR indicator, de Looze et al. (2011) find a scatter of a factor of 3, and Boselli et al. (2002) find a scatter of a factor of 10. Combining the SFR versus FIR luminosity relation from Kennicutt (1998) with the de Looze et al. (2011) SFR versus [C II] relation essentially requires a [C II]/FIR = 10^{-3} within a factor of 3. This holds true for about half of our sample.

What [C II] does directly measure is the cooling of neutral gas, as it is the main cooling channel for neutral gas. Thus, it measures the heating of neutral gas. The dominant mode of heating the neutral ISM is the photoelectric effect. Incident FUV photons with energies high enough to eject electrons from dust grains ($h\nu > 6$ eV) heat the gas via these photoelectrons, with a typical efficiency of 0.1%–1%, where efficiency is defined as the energy input to the gas divided by the total energy of the FUV photons absorbed by the dust grains. This efficiency is determined by the microphysics of the grains, particularly the work function, the photoelectric yield, and the charge of the grains (which is determined by the ratio of FUV fluxes to gas density, G_0/n). The [C II]/FIR ratio is interesting because it gives the efficiency of the photoelectric effect, since the numerator measures the energy that has gone into heating the gas and the denominator the energy absorbed by dust

grains. There are several possible theories that have been put forward to explain the observed variations in the [C II]/FIR ratio.

(A) In places where intense UV radiation leads to high values of G_0/n (where G_0 is the UV radiation flux and n is the density of gas), we should see hotter dust grains. We should also see a larger net positive charge on dust grains, since the balance between photoelectric (PE) ionization and recombinations results in higher positive charge for high values of G_0/n . The efficiency of photoelectric heating then decreases because of the higher electric potential of the grains (TH85). If the gas is heated less efficiently, we should see a proportionately lower cooling rate. Thus, we should see an anticorrelation between [C II]/FIR and dust temperature or FIR color (F60/F100). This trend was seen in nearby normal galaxies by M97 and M01. In Figure 3, we see that the [C II]/FIR ratio of high-redshift galaxies follows the same trends with F60/F100 as that of low-redshift galaxies, independently of their luminosities.

(B) The [C II] line may be optically thick or self-absorbed due to colder foreground gas. Such self-absorption is seen toward the galactic center and in the Galactic star formation region M17 (Boreiko & Betz 1997; Graf et al. 2012). This hypothesis seems to be supported by the correlation between a spatially compact mid-IR dust distribution and a suppressed [C II]/FIR ratio, seen for luminous infrared galaxies by Díaz-Santos et al. (2013). While compactness does make self-absorption more likely, it does not prove high optical depths in the [C II] line. In fact, a compact configuration of star-forming regions and the ISM also naturally leads to higher UV fluxes and higher dust temperatures and hence to the suppression of $L_{[\text{C II}]} / L_{\text{FIR}}$ by mechanism (A).

(C) Other possible explanations of low [C II]/FIR include (1) a scarcity of C+ due to the absorption of C ionizing flux by high columns of dust and (2) the suppression of [C II] emission when the density of neutral gas exceeds the critical density of $\approx 10^3$. Both these effects were discussed by Malhotra et al. (1997), Kaufman et al. (1999), Stacey et al. (2010), and others. In these two scenarios, [C II] deficiency is due not to a lower heating efficiency of the gas, but to the cooling of neutral gas via channels other than the [C II] fine structure line. In that case we should see some other lines, such as [O I] ($63 \mu\text{m}$), play a dominant role in the cooling of neutral gas. The observed anticorrelation between [C II]/FIR and dust temperature neither rules out nor supports these scenarios. Other lines, such as CO and [O I], would be needed to find out if [C II] deficiency indeed happens in high-density or low-ionization scenarios in galaxies (e.g., Kaufman et al. 1999; Malhotra et al. 2001). For nearby galaxies, the [O I] ($63 \mu\text{m}$) line does become brighter than [C II] at high F60/F100, but not enough to fully explain the trend of decreasing [C II]/FIR (Malhotra et al. 2001).

Stacey et al. (2010) pointed out that high-redshift galaxies do not follow the anticorrelation between [C II]/FIR and FIR luminosity seen for low- z samples. This is good news indeed, because it means that we can detect [C II] for high- z galaxies more easily. But even for nearby galaxies, the correlation between FIR luminosity and [C II]/FIR is weaker than the correlation between [C II]/FIR and F60/F100. The correlation coefficient for the former is $R = -0.6$ versus $R = -0.7$ for the latter. In fact, when we plot [C II]/FIR versus F60/F100, the high-redshift galaxies fall in the same sequence as the low-redshift galaxies, in that the cooler galaxies have higher [C II]/FIR in spite of having high luminosity.

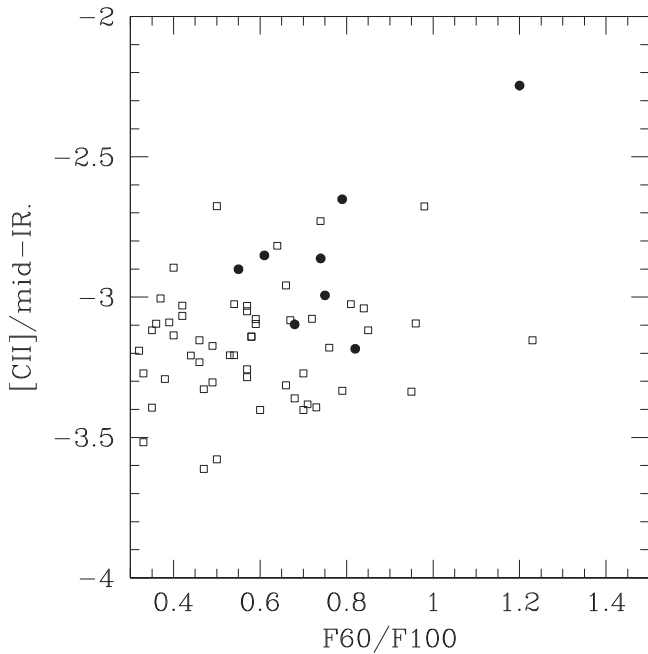


Figure 5. The ratio of [C II] line luminosity and mid-IR flux is plotted against F60/F100 for 8 high-redshift galaxies from the HELLO sample (filled circles) and 55 nearby galaxies from Helou et al. (2001; hollow squares). The MIR flux is taken to be the $7\ \mu\text{m}$ flux for the Helou sample and the observed $24\ \mu\text{m}$ flux for the high-redshift sample. The constancy of the [C II]/MIR ratio at high and low redshifts is further support for the hypothesis that PAH grains are dominant sources of photoelectric heating. The source with the highest [C II]/MIR is MS1512-cB58. It is 2-sigma off from the mean. Further investigation would be needed to figure out why this is an outlier.

It had been difficult to separate the dependence of [C II]/FIR on FIR luminosity and dust temperature in the low-redshift sample, since luminous infrared galaxies at low redshifts also show a high F60/F100 ratio (see Figure 4). At high redshifts though, we are able to probe only galaxies with relatively high luminosities, $\log(L_{\text{FIR}}) > 10.5$, even with the magnification boost due to lensing. But the main difference is that for the high-redshift sample the luminosity and temperature are not correlated. In other words, at low redshift, (almost) all highly luminous galaxies have warm dust, but at high redshifts, luminous galaxies show a range of colors in the FIR, including those that indicate cool dust. This has been pointed out with *ISO*, *SCUBA*, *Spitzer*, and *Herschel* data in several papers (Efstathiou & Rowan-Robinson 2003; Symeonidis et al. 2009; Elbaz et al. 2010; Hwang et al. 2010; Rujopakam et al. 2011; Díaz-Santos et al. 2013). Hailey-Dunsheath et al. (2010) did PDR modeling of MIPSJ1428 to infer a lower UV illumination of PDRs and deduced that the star formation was extended in size.

Before we conclude this discussion, it would be valuable to reconsider whether we should really expect [C II]/FIR to be constant. Very small grains and polycyclic aromatic hydrocarbons (PAHs) have a much higher efficiency of photoelectric heating than large grains (Watson 1972; Bakes & Tielens 1994; Weingartner & Draine 2001) because the photoelectron is likely to lose less energy as it works its way from the ejection site within the grain to the outside. About half of photoelectric heating comes from small grains/PAHs. Moreover, small grains maintain a high efficiency in the regime of high UV radiation intensity, because their recombination rate with electrons is higher. The rest of the incident photon energy absorbed by these small grains is radiated in the mid-infrared

since the PAHs and VSGs get stochastically heated to high temperatures. In this scenario, we should expect the ratio between the [C II] line and thermal emission from small grains in the mid-IR to show a constant ratio. The PAHs/VSGs are cooled by emitting in the mid-IR. The proportionality between MIR and [C II] fluxes was demonstrated by Helou et al. (2001) for nearby galaxies. In Figure 5 we show that high-redshift galaxies also follow the same proportionality, indicating that the photoelectric heating of the neutral gas is dominated by PAHs. Unfortunately, we have MIR fluxes for only a few high- z sources.

5. SUMMARY AND CONCLUSIONS

To summarize, our main conclusions in this study are as follows:

- (A) We detect the [C II] ($158\ \mu\text{m}$) fine structure line in 14 out of 15 lensed galaxies that we observed at $1 < z < 3$. We find three sources with [C II]/FIR $\geq 1\%$.
- (B) At both low and high redshifts, the dust temperature (indicated by FIR color) and not the FIR luminosity is the main determining factor for the [C II]/FIR ratio. Galaxies with warmer FIR colors show lower [C II]/FIR ratios.
- (C) At low redshifts, highly luminous galaxies tend to have warm dust, so the effects of dust temperature and luminosity are hard to disentangle. Luminous galaxies at high redshifts show a range of dust temperatures, making it possible to establish that [C II]/FIR correlates most strongly with dust temperature.
- (D) This anticorrelation (i.e., lower [C II]/FIR for higher F60/F100 ratios) is best explained with a scenario in which increased UV intensity leads to higher FIR luminosity and dust temperatures, but the gas heating does not rise proportionately due to lower photoelectric heating efficiency. It is also possible that lower [C II]/FIR arises not because the photoelectric heating efficiency is lower but because [C II] ceases to be a main cooling channel. In that case we should see other strong lines, such as [O I] ($63\ \mu\text{m}$), from PDRs.
- (E) The proportionality between the mid-IR dust continuum and the [C II] line flux holds for high-redshift galaxies, indicating that PAHs are dominant sources of photoelectrons that heat neutral gas.

Herschel is an ESA space observatory with science instruments provided by European-led Principal Investigator consortia and with important participation from NASA. We are grateful to the DARK Cosmology Centre in Copenhagen, Denmark; Nordea Fonden in Copenhagen; the Institute for Advanced Study in Princeton, NJ; and Princeton University's Department of Astrophysical Sciences for their hospitality during the completion of this work. We thank the staff at the NASA *Herschel* Science Center, and Adwin Boogert in particular, for their assistance and guidance with HIFI data. The authors would like to thank Gordon Stacey for discussions, the referee for careful readings of the manuscript, and the editor for their patience. This work has been supported by NASA through *Herschel* GO funding.

REFERENCES

- Allam, S. S., Tucker, D. L., Lin, H., et al. 2007, *ApJL*, 662, L51
 Appleton, P. N., Guillard, P., Boulanger, F., et al. 2013, *ApJ*, 777, 66

- Bakes, E. L. O., & Tielens, A. G. G. M. 1994, *ApJ*, **427**, 822
- Bayliss, M. B., Hennawi, J. F., Gladders, M. D., et al. 2011, *ApJS*, **193**, 8
- Bayliss, M. B., Wuyts, E., Sharon, K., et al. 2010, *ApJ*, **720**, 1559
- Belokurov, V., Evans, N. W., Moiseev, A., et al. 2007, *ApJL*, **671**, L9
- Bergvall, N., Masegosa, J., Östlin, G., & Cernicharo, J. 2000, *A&A*, **359**, 41
- Bertin, E., & Arnouts, S. 1996, *A&AS*, **117**, 393
- Boreiko, R. T., & Betz, A. L. 1997, *ApJS*, **111**, 409
- Borys, C., Blain, A. W., Dey, A., et al. 2006, *ApJ*, **636**, 134
- Boselli, A., Gavazzi, G., Lequeux, J., & Pierini, D. 2002, *A&A*, **385**, 454
- Capak, P., Carilli, C., Jones, G., et al. 2015, *Nature*, **522**, 455
- Carilli, C., & Walter, F. 2013, *ARAA*, **51**, 105
- Contursi, A., Poglitsch, A., Gracia Carpio, J., et al. 2013, *A&A*, **549**, A118
- Cormier, D., Madden, S. C., Hony, S., et al. 2010, *A&A*, **518**, L57
- Crawford, M. K., Genzel, R., Townes, C. H., & Watson, D. M. 1985, *ApJ*, **291**, 755
- Dale, D., Helou, G., Contursi, A., Silbermann, N. A., & Kolhatkar, S. 2001, *ApJ*, **549**, 215
- de Graauw, T., Helmich, F. P., Phillips, T. G., et al. 2010, *A&A*, **518**, L6
- de Looze, I., Baes, M., Bendo, G. J., Cortese, L., & Fritz, J. 2011, *MNRAS*, **416**, 2712
- Díaz-Santos, T., Armus, L., Charmandaris, V., et al. 2013, *ApJ*, **774**, 68
- Díaz-Santos, T., Armus, L., Charmandaris, V., et al. 2014, *ApJL*, **788**, L17
- Diehl, H. T., Allam, S. S., Annis, J., et al. 2009, *ApJ*, **707**, 686
- Efstathiou, A., & Rowan-Robinson, M. 2003, *MNRAS*, **343**, 322
- Elbaz, D., Hwang, H. S., Magnelli, B., et al. 2010, *A&A*, **518**, L29
- Fadely, R., Allam, S. S., Baker, A. J., et al. 2010, *ApJ*, **723**, 729
- Farrah, D., Lebouteiller, V., Spoon, H. W. W., et al. 2013, *ApJ*, **776**, 38
- Finkelstein, K. D., Papovich, C., Finkelstein, S. L., et al. 2011, *ApJ*, **742**, 108
- Fischer, J. 2000, in *ESA Special Publication 456, ISO Beyond the Peaks: The 2nd ISO Workshop on Analytical Spectroscopy*, ed. A. Salama et al. (Les Ulis: EDP), 239
- Förster Schreiber, N. M., Genzel, R., Bouche, N., et al. 2009, *ApJ*, **706**, 1364
- Frayer, D. T., Sanders, D. B., Surace, J. A., et al. 1999, *ApJL*, **514**, L13
- Graciá-Carpio, J., Sturm, E., Hailey-Dunsheath, S., et al. 2011, *ApJL*, **728**, L7
- Graf, U. U., Simon, R., Stutzki, J., et al. 2012, *A&A*, **542**, L16
- Griffin, M. J., Abergel, A., Abreu, A., et al. 2010, *A&A*, **518**, L3
- Hailey-Dunsheath, S., Nikola, T., Stacey, G. J., et al. 2010, *ApJL*, **714**, L162
- Heiles, C. 1994, *ApJ*, **436**, 720
- Helou, G., Khan, I. R., Malek, L., & Boehmer, L. 1988, *ApJS*, **68**, 151
- Helou, G., Malhotra, S., Hollenbach, D. J., Dale, D. A., & Contursi, A. 2001, *ApJL*, **548**, L73
- Hunter, D. A., Kaufman, M., Hollenbach, D. J., et al. 2001, *ApJ*, **553**, 121
- Hwang, H. S., Elbaz, D., Magdis, G., et al. 2010, *MNRAS*, **409**, 75
- Iono, D., et al. 2007, in *ASP Conf. Ser. 375, From Z-Machines to ALMA: (Sub)Millimeter Spectroscopy of Galaxies*, ed. A. J. Baker et al. (San Francisco, CA: ASP), 246
- Israel, F. P., & Maloney, P. R. 2011, *A&A*, **531**, A19
- Iverson, R. J., Swinbank, A. M., Smail, I., et al. 2013, *ApJ*, **772**, 137
- Kaufman, M. J., Wolfire, M. G., Hollenbach, D. J., & Luhman, M. L. 1999, *ApJ*, **527**, 795
- Kennicutt, R. C., Jr. 1998, *ApJ*, **498**, 541
- Kneib, J.-P., van der Werf, P. P., Knudsen, K. K., et al. 2004, *MNRAS*, **349**, 1211
- Koester, B. P., Gladders, M. D., Hennawi, J. F., et al. 2010, *ApJL*, **723**, L73
- Leech, K. J., Volk, H. J., Heinrichsen, I., et al. 1999, *MNRAS*, **310**, 317
- Lin, H., Buckley-Geer, E., Allam, S. S., et al. 2009, *ApJ*, **699**, 1242
- Luhman, M. L., Satyapal, S., Fischer, J., et al. 1998, *ApJL*, **504**, L11
- Luhman, M. L., Satyapal, S., Fischer, J., et al. 2003, *ApJ*, **594**, 758
- Madden, S. C. 2001, in *ESA Special Publication 460, The Promise of the Herschel Space Observatory*, ed. G. L. Pilbratt et al. (Les Ulis: EDP), 159
- Madden, S. C., Geis, N., Genzel, R., et al. 1993, *ApJ*, **407**, 579
- Magnelli, B., Lutz, D., Santini, P., et al. 2012, *A&A*, **539**, 155
- Maiolino, R., Caselli, P., Nagao, T., et al. 2009, *A&A*, **500**, L1
- Malhotra, S., Helou, G., Stacey, G., et al. 1997, *ApJL*, **491**, L27
- Malhotra, S., Hollenbach, D., Helou, G., et al. 2000, *ApJ*, **543**, 634
- Malhotra, S., Kaufman, M. J., Hollenbach, D., et al. 2001, *ApJ*, **561**, 766
- Mellier, Y., Fort, B., Soucail, G., Mathez, G., & Cailloux, M. 1991, *ApJ*, **380**, 334
- Nguyen, H. T., Schulz, B., Levenson, L., et al. 2010, *A&A*, **518**, L5
- Ofek, E. O., Seitz, S., & Klein, F. 2008, *MNRAS*, **389**, 311
- Pello-Descayre, R., Sanahuja, B., Soucail, G., Mathez, G., & Ojero, E. 1988, *A&A*, **190**, L11
- Pierini, D., Leech, K. J., Tuffs, R. J., & Volk, H. J. 1999, *MNRAS*, **303**, L29
- Pilbratt, G. L., Riedinger, J. R., Passvogel, T., et al. 2010, *A&A*, **518**, L1
- Pineda, J. L., Langer, W. D., Velusamy, T., & Goldsmith, P. F. 2013, *A&A*, **554**, 103
- Poglitsch, A., Waelkens, C., Geis, N., et al. 2010, *A&A*, **518**, L2
- Rhoads, J. E., Malhotra, S., Allam, S. S., et al. 2014, *ApJ*, **787**, 8
- Riechers, D. A., Bradford, C. M., Clements, D. L., et al. 2013, *Nature*, **496**, 329
- Rigby, J. R., Marcillac, D., Egami, E., et al. 2008, *ApJ*, **675**, 262
- Roelfsema, P. R., Helmich, F. P., Teyssier, D., et al. 2012, *A&A*, **537**, A17
- Rujopakarn, W., Rieke, G. H., Eisenstein, D. J., & Juneau, S. 2011, *ApJ*, **726**, 93
- Rujopakarn, W., Rieke, G. H., Papovich, C. J., et al. 2012, *ApJ*, **755**, 168
- Saintonge, A., Lutz, D., Genzel, R., et al. 2013, *ApJ*, **778**, 2
- Smith, B. J., & Madden, S. C. 1997, *AJ*, **114**, 138
- Stacey, G. J., Geis, N., Genzel, R., et al. 1991, *ApJ*, **373**, 423
- Stacey, G. J., Hailey-Dunsheath, S., Ferkinhoff, C., et al. 2010, *ApJ*, **724**, 957
- Symeonidis, M., Page, M. J., Seymour, N., et al. 2009, *MNRAS*, **397**, 1728
- Tielens, A. G. G. M., & Hollenbach, D. 1985, *ApJ*, **291**, 722
- Unger, S. J., Clegg, P. E., Stacey, G. J., et al. 2000, *A&A*, **355**, 885
- Venemans, B. P., McMahon, R. G., Walter, F., et al. 2012, *ApJ*, **751**, L25
- Watson, W. D. 1972, *ApJ*, **176**, 103
- Weingartner, J. C., & Draine, B. T. 2001, *ApJ*, **563**, 842
- Wolfire, M. G., Tielens, A. G. G. M., & Hollenbach, D. 1990, *ApJ*, **358**, 116
- Yee, H. K. C., Ellingson, E., Bechtold, J., Carlberg, R. G., & Cuillandre, J.-C. 1996, *AJ*, **111**, 1783